5-1-2001

New approaches to processing nanoparticles and nanostructures

Mathew M. Maye

New Approaches to Processing Nanoparticles and Nanostructures

Mathew M. Maye

Department of Chemistry, State University of New York at Binghamton,

Binghamton, New York 13902

Accepted in partial fulfillment of the requirements for
Distinguished Independent Work in Chemistry
State University of New York at Binghamton

May 1, 2001

Professor Chuan-Jian Zhong C.J. Zhong **May 1, 2001**
Advisor
Department of Chemistry

Professor M. Stanley Whittingham M. Stanley Whittingham **May 1, 2001**
Department of Chemistry

Professor David C. Doetschman David C. Doetschman **May 1, 2001**
Department of Chemistry

Abstract

The study of nanoparticles is an emerging field of nanoscience and nanotechnology. A challenging issue is how deliberate tailoring and processing of the nanoscale materials can lead to well-defined and functional nanostructures. In this thesis, we explore new strategies of nanoscale design and processing to address the challenge.

A core-shell chemical processing route towards fabrication of functional composite nanomaterials with defined sizes, shapes, compositions and surface properties is demonstrated. New findings of an investigation of thermally-activated core-shell reactivities of nanoparticles in solutions are described. Gold nanoparticles of ~2-nm core size with thiolate monolayer encapsulation were chosen as a model system for delineating design and processing parameters. We have demonstrated a remarkable evolution of the preformed particles in solutions towards monodispersed larger core sizes (5~10 nm) with well-defined shape and facet morphologies. The particles thus evolved were encapsulated with the thiolate shells, and exhibited striking propensities of forming long range ordered arrays.

While temperature-driven crystal growth is known for bare particles, the evolution of the encapsulated nanoparticles in solutions into well-defined morphologies represents an intriguing pathway for size and shape control. It is further demonstrated that solution-annealing treatment in the presence of encapsulating thiols could lead to highly monodispersed nanoparticles. Insights into shell desorption, core coalescence and shell re-encapsulation have been provided by detailed examination of evolution temperature, thiolate chain length and core alloy composition. TEM, FTIR, UV-Visible, XRD, techniques were utilized for morphological and structural characterizations. The implication of our findings to the development of abilities in chemical processing nanoparticle size, shape and surface properties is also discussed.

Table of Contents

Overview

A rapidly-emerging frontier in science involves the processing and characterization of materials and structural properties at the nanoscale. One intriguing class of nanoscale materials is metallic and semiconductive nanoparticles in the range of 1-100 nm. The significance of nanoparticle materials is closely linked to a number of structural attributes. First, the chemical composition of the nanoparticle plays an important role in the electronic properties. Second, the size and shape of the nanoparticle are crucial for the construction of functional architecture. And third, the surface properties of the nanoparticles determine the stability and interfacial reactivities. One major problem facing the ultimate industrial manufacturing of nanoscale materials is the lack of abilities to fabricate these particles in large quantities with controlled size, shape, composition, and surface properties. The search for the abilities has attracted enormous interests in research laboratories around the world.

The nanoscale particles serve as ideal building blocks to construct functional platforms via "bottom up" strategies. Of many nanoscale materials synthesized or fabricated in recent years, nanorods and nanotubes have shown remarkable characteristics. Semiconductive, metallic and magnetic particles ranging from 100-1000 nm have been abundantly studied over the past decade [3-5]. Gold particles in particular have been widely studied largely due to their stability and the relative ease of preparing small sizes [6-10]. Gold colloids, dating back to the early studies of Faraday[11], showed many interesting properties for electronic and optical applications. The driving force for the recent increasing interest in gold and other metallic nanoparticles is largely due to the recognition of novel electronic and interfacial properties emerging as metal particles leave the "bulk" and enter into a domain of only a few nanometers.

A difficult problem encountered for nanoparticle systems at the nanoscale dimension (1 billionth of a meter) is the propensity of nanoscale core-to-core aggregation. To overcome this obstacle, gold nanoparticles were recently synthesized with protective organic shells. These "core-shell" nanoparticles can be synthesized to produce particles in the range of 2-50 nm [8]. One intriguing class of core-shell systems receiving enormous research interest over the past seven years is gold or other metallic cores encapsulated with thiolate monolayer shells [8-10]. Such nanoparticles (a few nm in diameter) can be synthesized by two-phase protocol developed first by Schiffrin and co-workers [8]. This class of nanoparticles takes advantages of self assembled thiolate monolayers (SAM) on gold that have been extensively studied over the past decade [12-15]. These nanoparticles have demonstrated potential applications in microelectronics, optic devices, magnetic materials, catalysis and molecular recognition. While the particles are quite monodisperse in comparison with particles synthesized without the monolayer shells, the need for highly-monodispersing and highly-shaped particles continues to pose challenging issues to researchers. The precise control over reactivity in the synthetic process is a key. The use of sodium borohydrate to reduce $AuCl_4^-$ to Au^0 and the competition between Au^0 aggregation and thiolate encapsulation involve complicated interfacial processes. The varied sizes and shapes pose limitations to the potential applications of these particles. In addition, the high cost associated with the use of large amount of solvent in synthesis limit the scope in terms of scale-up applications. The development of simple and highly effective processing methods constitutes an important challenge for the ultimate industrial manufacturing of nanoscale materials.

We have recently explored new synthetic and processing strategies to address the above challenging issues. In one strategy, we focused on processing of pre-synthesized nanoparticles, which is termed as thermally-activated core-shell processing [16]. It involves manipulation of the core-shell reactivity to process nanoparticle size, shape and surface properties. The elevation of temperature beyond both the melting point of nano-dimensioned gold and the organic solvent boiling point can lead to desorption of the thiolate shell, core-core coalescence, and re-encapsulation. These core-shell reactivities result in core size evolution to larger-sized particles (e.g., 5 nm size). Further "solution annealing" and other processing parameters such as heating solution composition and temperatures could lead to highly-monodispersing and highly faceted nanocrystals. Importantly, the evolution in shape and surface properties can also be manipulated by core-shell structural tailoring[16b].

A critical question is why the study of nanoparticles and the control of size, shape and surface properties are so important. This question is on the mind of many researchers, government agencies and industrial leaders due to various concerns or interests in their particular applications. There are a number of important attributes for studying nanoparticle synthesis and processing in terms of size, shape and surface properties. A few examples are outlined below, each showing the importance of size, shape and surface processing and tailoring.

First of all, many researchers, including our research group, hope to harness the novel properties of nanoparticles and use them as functional materials. We explored the "bottom up" approach towards the creation of novel nanoscale building blocks whose interfacial reactivities are tailorable. While conventional routes towards miniaturization involve "top-down" masking lithography, which utilize very specialized facilities and sophisticated instrumentation. This limits the access of the technology to researchers. The recent development in "soft-lithography", i.e., micro-contact printing, is a new step towards miniaturization. In comparison with the "top-down" approach, the "bottom-up" approach often involves atom by atom, nanoparticle by nanoparticle, construction. Interestingly, such nanoscale manipulation can be done in the conventional laboratory, with controllability in chemical manipulation and careful characterization. In our recent work, we explored the nanoscale "bottom up" approach towards novel functional nanostructures which involves molecules, nanoparticles and interfacial reactivity.

One interesting bottom-up approach utilizes self-assembly and interparticle combination. We are able to create nanostructured thin films as sensor materials that can selectively and sensitively target different analytes. In addition to harnessing the structural properties of thiolate-encapsulated gold nanoparticles, we can fine-tune the nanostructured properties for a specific analytical application. Because the interfacial interaction and reactivity of nanoparticles are highly dependent on size, shape and surface properties, the ability to process size, shape and surface property is needed in developing nanostructured sensor materials.

Among many of the research projects that I have participated in the past several years, the development of novel analytical platforms involved exploitations of the many facets of nanostructured materials. One example was a new technique towards construction of thin films via molecular crosslinkers. The "one step exchange-crosslinking-precipitation technique" developed recently in our laboratory created many possibilities for potential applications[17]. By manipulating crosslinking chemistry of functionalized molecules including covalent- and hydrogen-binding properties, we created a thin film that has novel biomimetic ion-gating properties [18]. We showed that the thin film systems could be "fine-tuned" by changes in solution pH. Interestingly, electrochemical ion-gating properties that mimic biological membrane processes were demonstrated for a number of different redox probes. Such properties are strongly dependent on the size and surface properties of the nanocrystal cores and the structure of organic shells.

We have also demonstrated that the nanostructured thin film system can also undergo secondary "building up." The process involves the derivertization of functional groups in the thin film. Here, we take advantage of the end-group of the carboxylic acid-functionalized crosslinkers. By an interfacial dehydration reaction, we successfully converted the hydrogen-bonded network to a covalent anhydride structure. This approach may be proven viable for studies of many different analytes including biological species [19]. Again, the size and surface properties of the nanoparticles were found to be important in the interfacial reactivity.

Novel electrochemical properties of nanoparticles have also been demonstrated which may have potential applications beyond analytical chemistry. We found recently that core-shell self-assembled gold nanoparticles showed catalytic activities towards CO and methanol electrooxidation upon catalytic activation [20]. Gold catalysis, due to the recent discovery of catalytic properties at bare nanosized gold colloids supported on oxides [21], is receiving increasing interest. The encapsulation and small core size of our approach may lead to poison-resistant and cost-effective fuel cell catalysts. The catalytic activity was found to be strongly dependent on the size, shape and surface properties of the nanocrystal cores.

One of our more recent interests involves the use of atomic force microscopy to probe nanoscale chemistry in the nanostructured materials. We are interested in creating nano or micro analytical "addresses" that can be utilized as imaging-based chemical sensors with built-in nano/micro internal standards. We have developed a method that involves surface "patterning" via micro-contact printed thiolate monolayers and nanoparticle assembly via "one step method" [22]. This process can be integrated into all of the above systems to monitor morphological changes during interfacial reactions. Preliminary insights into nanoscale structure-reactivity relationship demonstrate that the use of well-defined nanocrystal size and shape should facilitate the nanoscale probing.

Throughout all of these investigations in the past several years and based on the current understanding of the nanoparticle processing chemistry, it is becoming increasingly clear that the ability to control size, shape and surface properties of nanoparticles is one of the most challenging issues. As a starting point in the exploration of core-shell nanoparticles, we aimed at developing new strategies for processing core-shell nanoparticles in terms of size, shape and surface properties. The focus of this thesis is the development of thermally-activated processing strategy for precise control of nanoparticle size and surface properties. The design parameters needed to manipulate the size, shape, and surface properties of the gold and alloy nanoparticles are discussed. Our strategy is capable of inducing size and shape change of composite nanoparticles in solutions towards monodispersed larger core sizes with well-defined and highly-faceted morphologies . The nanoparticles thus processed were characterized using a number of techniques, including transmission electron microscopy, X-ray diffraction, UV-visible spectrophotometry, FT-infrared spectroscopy, and atomic force microscopy.

Introduction to Synthesis and Processing of Nanoparticles

When thinking of the possibility of heat induced evolution, we first examined relevant literature work, and then assessed the chemical parameters related to such a process.

Nanoparticles of various core sizes (2 to 6 nm range) can be produced by manipulation of the synthetic precursor ratios, e.g., thiol-to-gold ratio.[8-15] The synthesis of smaller-sized particles, e.g., ~2 nm average core sizes, is relatively easy by using large thiol-to-gold ratios, whereas larger-sized nanoparticles can be formed by decreasing the ratio. This type of manipulation is effective, but requires extensive synthetic work to produce particles in different sizes.

There have also been a number of approaches to developing size and shape control abilities. The two-phase synthesis carried out at temperatures between -78 and 90 ^{0}C was demonstrated to produce 2~3 nm core sizes with different size dispersity.[15] Methods including seeding,[7] templating,[7,23] the use of shape-inducing agent, [23-24] and fractional separation [25] were experimentally demonstrated to be successful to various degrees for producing shapes in some nanoparticle systems. Fundamentally, however, relatively little is known for the precise control of shapes and sizes for the composite nanomaterials. The concept of heating-induced growth of metal or metal oxide particles or crystals is not new (e.g., traditional Ostwald ripening).[26] Such treatments were utilized for systems supported on substrates in processes involving nucleation, dissolution and growth.[27-28] In view of the molecular and crystal natures of the core-shell systems, size and shape formation is inherently a dynamic process, and an evolution may occur as a result of changes in chemical potentials of the particles and the environmental components. To our knowledge, while the synthesis of thiolate-encapsulated particles at elevated temperatures has been reported,[15] heating treatment of preformed thiolate-encapsulated nanoparticles in solutions had not yet been studied for inducing size and shape changes. We noted two recent studies of temperature dependence on the stability of bare gold nanoparticles [29] and gold nanorods in solutions.[23] The finding of a gradual decrease of the aspect ratio for gold nanorods was attributed to the thermal reshaping effect.

Scheme 1 depicts our hypothesis for core-shell reactivities of the alkanethiolate-capped gold nanoparticles under thermal activation. In this scheme, larger core sizes result from an evolution of the smaller-sized starting particles via sequential shell desorption, core coalescence and shell re-encapsulation. This route had not been explored in previous studies as processing strategy for core-shell nanoparticle systems.

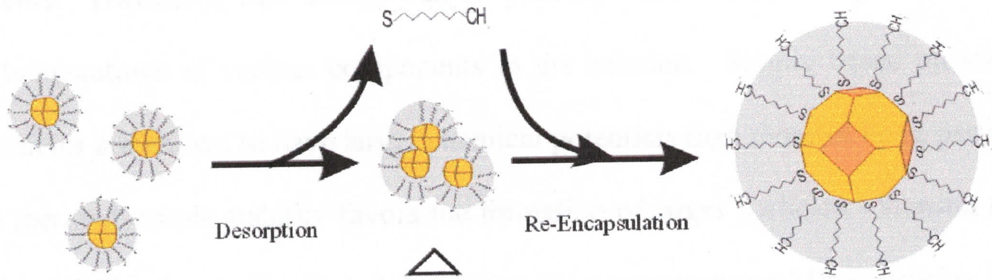

Scheme 1. A schematic illustration of the core-shell reactivities in the thermally-activated size and shape evolution process of thiolate-capped nanoparticles.

We believe that thermally-activated core-shell reactivities can be explored as a useful strategy for inducing changes in size, shape and surface properties of nanoparticles from solutions of preformed thiolate-capped gold nanoparticles. We describe our findings of such an explorations, focusing on factors controlling the core-shell reactivities for the processing of sizes, shapes and surface properties. Gold nanoparticles encapsulated with alkanethiolate monolayers synthesized by Schiffrin's two-phase protocol were studied as a model system. This study is also expanded to systems of core-shell nanoparticles with different metallic and alloy core compositons.

Basic Considerations of Boiling and Melting Temperatures of Nanoparticle Solutions

This section describes our considerations of the basic correlation of temperatures with processes involving melting and boiling phenomena. For a solution containing nanoparticles as solute and an organic solvent (in this work), the chemical potential (μ) can be described by

$$\mu_i = \mu^*_i + RT\ln x_i \quad\text{.........(1)}$$

in which x_i represents the mole fraction of solute or solvent component. The thermodynamic stability of the solution is closely linked to the chemical potentials for each of the components. Thermally, this linkage can be partially reflected by changes of melting and boiling temperatures of various components in the solution. Simply based on size effect, small particles are known to have larger chemical potentials than those of large particles, and thus the thermodynamic stability favors the formation of larger particles. Starting from this fundamental basis, theories predicted that the melting temperature of fine particles decreases as a function particle size, and that the boiling temperature rises as a function of mole fractions, both of which are described next.

An early thermodynamic model describing melting curve for fine metal particles was reported by Buffat and co-workers,[30-31] which relates the melting point to that of its bulk metal by the equation,

$$\frac{T_d - T_\infty}{T_\infty} = -\frac{4}{\rho_s L d}\left[\gamma_s - \gamma_l\left(\frac{\rho_s}{\rho_l}\right)^{2/3}\right] \quad\text{.........(2)}$$

where T_d and T_∞ are melting temperatures of the particle and the bulk solid, respectively, d is the diameter of the particle, ρ_s and ρ_l are the density of the solid and the liquid, γ_s and γ_l are the surface energy of the solid and the liquid, and L is the heat of fusion of the solid. The theoretical model predicts a basic trend, i.e., a decrease of the melting point with decreasing the particle size, as illustrated in Figure 1A. While the temperature profile predicted by the model was higher than experimental values, improved models indeed showed a better agreement with experiments.[26,31] The key conclusion is that the melting point for the nanoparticles is much lower than that for the bulk. We consider the decrease of melting point as a function of particle size as an opportunity for us to conduct the manipulation of nanoparticle size and shape under significantly-reduced heating temperatures. This means that we can use regular solvent with nanoparticles dissolved and mild temperature settings to carry out the heating process. As will be shown later, the actual temperature range, as indicated by the square in the plot, indeed allows us to induce size and shape evolution of the core-shell nanoparticles in solutions.

On the other hand, the overall temperature of a solution is limited by its boiling point (T_b). The change of T_b constitutes thus another factor for the basic consideration. As is well known for solution systems, T_b can be related to the mole fraction of the solvent (or the solute) by the relation derived under certain assumptions [32]

$$\frac{1}{T_b} = -\frac{R}{\Delta H}\left[\ln x_A - \frac{\Delta H}{R}\frac{1}{T^*}\right] \qquad (3)$$

where T^* is the boiling point of pure solvent, x_A is the mole fraction of the solvent, and ΔH is the associated enthalpy change. This equation predicts that the boiling point of the solution rises as a function of the concentration of the solute, as shown by the plot of T_b vs. x_A in Figure 1B. As will be described in the following sections, our operating temperatures are close to the values indicated by the horizontal dashed line in Figure 1.

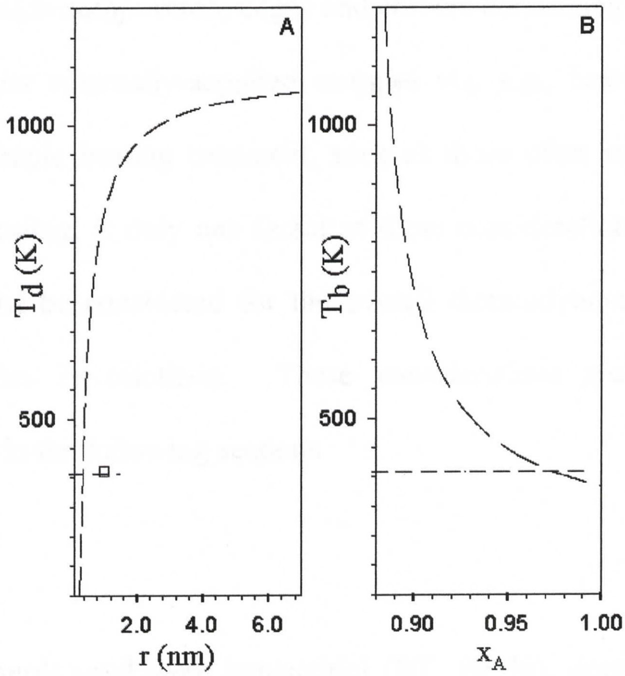

Figure 1. Theoretically calculated curves: (A) The melting temperature of gold nanoparticles as a function of particle radius based on eqn. 2. The parameters used were ρ_s=19,000 kg/m^2 and ρ_l=17,280 kg/m^2, γ_s=0.9 J/m^2 and γ_l =0.74 J/m^2, and L =53,800 J/kg. (B) The boiling temperature as a function of the mole fraction of the solvent based on eqn. 3. ΔH of toluene, 38 kJ/mole, was used

Both parameters, T_d and T_b, for a solution containing nanoparticles as solute are therefore closely linked to the particle size and concentration. These theoretical linkages constitute the basis for the concept of temperature-manipulated size and shape evolution in solutions of thiolate-encapsulated gold nanoparticles. Further, in an analogy to the usual high-temperature annealing, we anticipate that processes such as core coalescence and phase transitions, and reactivities such as thiolate desorption and re-adsorption may lead to changes in particle sizes and shapes. This type of changes can be related to the stability of different crystal facets, usually with (111)>(100)>(110) reflecting the order of surface free energy.

However, positive or negative contributions to these energies also include chemisorption of thiolates, changes of solution composition, edges and corners connecting the facets, and size and shape evolution under externally-supplied energies via, e.g., heating treatment. We emphasize here that a simple heating treatment, such as those often reported for Ostwald ripping and thermal annealing, is only one factor in these considerations. All the relevant solution components must be considered for the overall thermodynamic evolution of the encapsulated nanoparticles in solutions. These considerations are dispersed in our discussions of the results in the following sections.

Experimental Section

Chemicals. The thiols used were butanethiol (BT, 99+%), decanethiol (DT, 96%), dodecanethiol (DDT, 98+%), and octyldecanethiol (ODT, 98.5+%). The gold compound was hydrogen tetracholoroaurate ($HAuCl_4$, 99%). The organic salts used were tetraoctylammonium bromide (TOABr, 99%) and tetrabutylammonium bromide (TBABr, 99%). The reducing agent was sodium borohydride ($NaBH_4$, 99%). Other chemicals included toluene (Tl, 99.8%), hexane (Hx, 99.9%), ethanol (EtOH, 99.9%), and potassium bromide (KBr, 99+%). All chemicals were purchased from Aldrich and used as received. Water was purified with a Millipore Milli-Q water system.

Synthesis. The 2-nm gold nanoparticles encapsulated with alkanethiolate monolayer shells were synthesized by pre-mentioned standard two-phase method.[8] Briefly, $AuCl_4^-$ was first transferred from aqueous $HAuCl_4$ solution (10 mM) to toluene solution by phase transfer reagent TOABr (36 mM). Thiols, e.g., DT, was then added to the solution (21 mM) at a DT/Au mole ratio of 2:1. An excess (12x) of aqueous reducing agent ($NaBH_4$) was slowly added into the solution. The reaction was allowed proceed under stirring at room temperature for 4 hours, producing a dark-brown solution of DT-encapsulated nanoparticles. The solution was subjected to solvent removal in a rotary evaporator (at ~50^0C) followed by multiple cleanings using ethanol and acetone to purify the 2-nm sized particles, or used to induce size and shape evolution in the heating treatment experiments for size evolution. The 2-nm particle product appeared black and waxy.

The synthesis of gold alloy nanoparticles of an average core size ~3.5 nm, Au-Ag and Au-Pt, followed the procedures reported recently [33]. The Au-Ag nanoparticles were synthesized with DT encapsulation, whereas the Au-Pt was synthesized with DDT encapsulation. Briefly, the Au-Ag particles were synthesized in a 1:4 feeding ratio of $HAuCl_4$ to $AgNO_3$ dissolved in 25 mL of water. This solution was then added to a toluene solution of TOA^+ similar to the synthesis of gold nanoparticles. DT was then added to this solution followed by adding $NaBH_4$ (dropwise), resulting in a dark brownish solution containing the Au-Ag alloy nanoparticles. Au-Pt nanoparticles were synthesized in a similar manner but using a 1:1 ratio of $HAuCl_4$ to $K_2Pt_2Cl_6$, and DDT encapsulating thiol. The resulting nanoparticle solution appeared black

Processing. The heating treatment was performed with solutions of the pre-formed 2-nm nanoparticles in a temperature range from room temperature up to 160 °C. Two types of solvent were used. The first was a toluene solvent. The solution of the 2-nm particles directly resulted from the synthesis was either heated to the boiling point of the solvent (110 ^{0}C), or pre-concentrated by a factor of 15 before the subsequent heating at higher temperatures. The second type of solvent was a molten salt solvent, i.e., quaternary ammonium salts such as TOABr. The pre-formed 2-nm particles were dissolved in the molten salt (e.g., TOABr) for heating to the required temperature. In both cases, the solution was heated in a silicone oil bath with controlled temperature. The bath temperature was maintained at a constant temperature between 150 ^{0}C in the entire heating process. The temperatures both in the oil bath and in the sample solution were measured either using a thermometer or a thermocouple probe. The latter was connected to a computer-interfaced multimeter (Extech 380282) for direct monitoring of the temperature changes during the heating process. The bath temperature was higher than the sample temperature by ~20 ^{0}C before an apparent color change (i.e., size evolution) occurs, and was ~10 ^{0}C higher than the sample temperature when the color change occurs. When the temperature was elevated to above the boiling point of the solvent, the solution boiling was evident, and maintained during the entire heating process. The final products were subjected to cleaning cycles via suspension in ethanol and acetone and centrifugation for at least 4 times to ensure a complete removal of solvent and any possible by-products. The evolved particle product appeared gray and powdery.

Instrumentation. Infrared spectra were acquired with a Nicolet 760 ESP FT-IR spectrometer that was purged with boil-off from liquid N_2. The spectrometer was equipped with a liquid nitrogen-cooled HgCdTe detector. The nanoparticle powder sample was mixed with KBr powder and ground into fine powders. The powders were pressed into pallet at 15000 psi. The solution sample was measured using a thin-layer (0.5 mm) IR cell. The IR spectra were collected over the range of 400-4000 cm^{-1}.

UV-Visible (UV-Vis) spectra were acquired with a HP 8453 spectrophotometer. Nanoparticle samples were dissolved in hexane. The spectra were collected over the range of 200-1100 nm.

Transmission electron microscopy (TEM) was performed on Hitachi H-7000 Electron Microscope (100 kV). The nanoparticle samples dissolved in hexane or toluene solution were drop cast onto a carbon-coated copper grid sample holder followed by natural evaporation at room temperature.

X-Ray Diffraction (XRD) powder analysis was performed with a Philips X'PERT-MRD X-ray diffractometer. The powder sample was either smeared onto a glass holder (for 2 nm particles) or supported on vacuum grease (Dow Corning) on a glass substrate (for the larger sized particles).

Results and Discussion

The description and discussion of our results are divided into two parts. In the first part (Part I), we present the results to demonstrate the viability of the thermally-activated core-shell processing strategy. The evolution of size and shape of monolayer-capped gold nanoparticles is assessed. In the second part (Part II), we show the results to demonstrate the manipulation of the core-shell reactivities during the processing. Effects of solution annealing, shell chain length, and core-composition on the size, shape and surface properties of the processed particles are examined .

Part I. Thermally-Activated Size and Shape Evolution of Core-Shell nanoparticles

In the following sub-sections, we first present the results to assess the heating conditions and to discuss the induced evolution in terms of the melting, boiling, composition, and coalescencing parameters. We then present the TEM, IR, UV-Vis and XRD characterization data on the nanoparticle core sizes, shapes, crystallinities, and shell structures before and after the evolution. The results are also discussed in the context of developing an understanding of size and shape control for the core-shell nanomaterials.

Assessment of the Heating Conditions. We have studied a series of heating conditions including temperature, composition, and heating time length for solutions of the preformed nanoparticles. While the characterization data will be presented in the next section, this section first assesses two key conditions for the observed evolution of nanoparticles under heating treatment. The first is the necessity of pre-concentration of the pre-formed nanoparticles in solution. For example, the solution directly resulted from the nanoparticle synthesis contained ~40 μM of the DT-encapsulated nanoparticles (2-nm core size), 40 mM of TOA^{+} and 20 mM of DT. A direct heating of this solution at its boiling point (110 ^{0}C) for 5 hours did not induce any apparent change of the particles, which was evidenced by the un-changed solution color and identical UV-Vis spectra before and after the heating. This observation itself was remarkable because the encapsulated nanoparticles of this core size was shown to be stable even up to this temperature, unlike situations for non-thiolate encapsulated systems which displayed gradual changes of color or spectral properties at much below this temperature. In contrast, by pre-concentrating the solution to ~15 times of the original concentrations, i.e., a 600 μM of the particles, 600 mM of TOA^+ and 300 mM of DT, the continuous heating led to a further temperature rise from the boiling point of toluene up to 138 ±2 °C. At this temperature, a significant color change occurred from brown to dark red. This color change involved a size evolution as confirmed by TEM, UV-Vis and XRD data that are presented in following sections. Qualitatively, the preconcentration condition is consistent with the basic considerations on melting and boiling temperatures of nanoparticle solutions, as discussed in the early section. It has the initial effect of raising the boiling point of the sample. The pre-concentrated solution has a lower solvent fraction (x_A) and can thus be brought to a higher temperature, at which desorption, melting and coalescing processes or reactivities can be induced. During the evolution process, however, both the pre-concentration and the reactions contribute to the overall increase of the boiling point because the particle size evolution gradually changes the mole fractions of both solute and solvent. This is reflected by the gradual change of the sample temperature in figure 2. That is, the boiling point is not higher right away upon mixing and heating the concentrated components.

The second condition is the necessity for the presence of TOA^+ component in the solution. In our initial experiments, the nanoparticle solution was directly obtained from the resulting synthesis solution that contained TOA^+ and unreacted thiols. It turned out that the TOA^+ species present in the solution was an important component for the evolution. This assessment was confirmed by testing a solution containing only nanoparticles that had been pre-purified. The heating of the solution showed no signs of particle evolution. In contrast, an addition of TOABr together with thiols into the purified solution showed the color change. This result strongly supports the involvement of the quaternary ammonium salt in the evolution process. The addition of thiols to purified nanoparticle solution did not induce any observable color change, but its presence was important for ensuring encapsulation of the evolved nanoparticles.

An assessment of these observations therefore led us to the conclusion that the decrease of the solvent mole fraction for reaching a higher evolution temperature and the presence of the tetraalkylammonium salt for achieving a polar and hydrophobic environment for the evolution were two key factors. It is known that TOABr is a good low-temperature organic molten salt (the melting point for pure TOABr is ~100 ^{0}C).[34] The nanoparticles are soluble in this solvent. The highly-hydrophobic octyl chains provide the environment for stabilizing the intermediate nanoparticles during the evolution process. The fact that the use of less hydrophobic quaternary ammonium such as TBABr as molten salt could not produce any significant evolution was supportive of the above argument. The reason is largely due to the insolubility of the thiolate-encapsulated nanoparticles in the less hydrophobic molten salt. Clearly, the hydrophobic TOA^+ enabled a better mixing environment for the nanoparticles encapsulated with organic alkanethiolate shell. On the other hand, the hydrophobicity constituted only part of the environment for the evolution, because the use of hexatriacontaine (non-salt organic solvent) and ethylbenzene (higher boiling point) showed no signs of any observable evolution. Hence, we believe that it is likely that the ionic charge or polarity of TOA^+ provides another part of the environment for stabilizing the intermediate charged or polar species in the evolution process such as quasimelted nanoparticle cores and desorbed shell thiolates.

To further assess the involvement of desorption and coalescence processes in the heating-induced nanoparticle evolution, the temperature change as a function of time was monitored. Figure 2 shows two representative sets of temperature profiles determined during the heating process of the DT-encapsulated nanoparticles (2-nm core size) in two types of solution conditions.

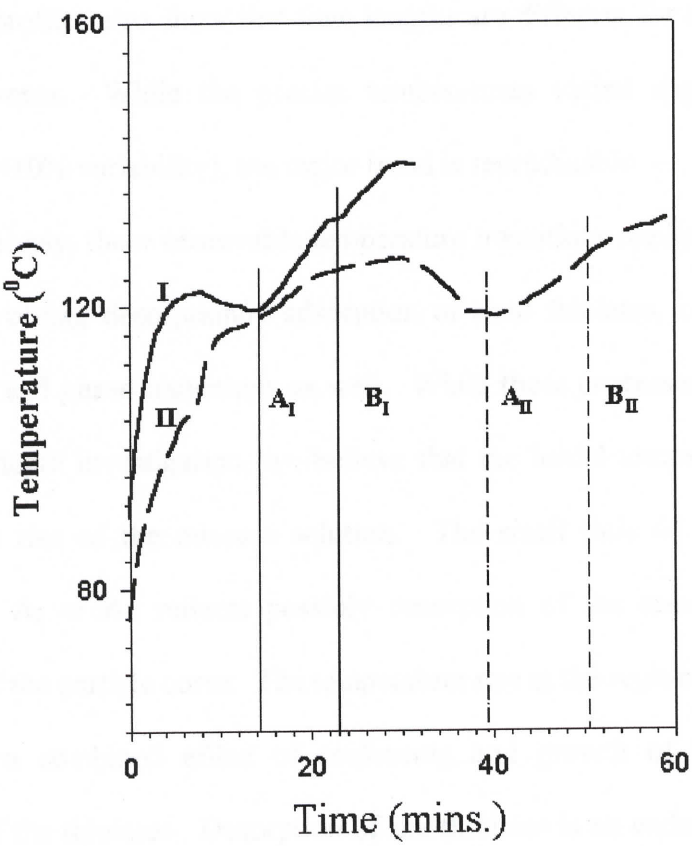

Figure 2. Temperature profiles in the heating process for the DT-encapsulated 2-nm Au nanoparticles dissolved in solutions. Curve I: in toluene solvent. Curve II: in the molten TOABr solvent.

Curve I is obtained for a toluene solution with pre-concentrated nanoparticles. Curve II is recorded for TOA^+ molten salt solution with dissolved nanoparticles. As is evident in these curves, the data reveal an initial rise of the temperature to above the boiling point of the solvent; this rise is followed by a small but observable fall of the temperature before a second rise to a temperature of ~138 ^{0}C. The evolution of the particle sizes, as reflected by the solution color progression, was observed near the temperature of 138 ^{0}C. Upon prolonged heating at this temperature, the solution was found to evolve from brown to light red to dark red to purple and eventually to a less-soluble or insoluble product. The temperature profiles also show that time lengths are different for the temperature changes in the two solvents. While the precise temperatures varied slightly from experiment to experiment (<10% variability), the major trend is reproducible.

Qualitatively, these observable temperature transitions may partially be associated with processes involving desorption/re-adsorption of shell thiolates, coalescence and growth of particle core and phase transitions as well. While these processes are complex and are still under an in-depth investigation, we believe that the initial temperature plateau reflects the boiling point rise of the mixture solution. The small falls of temperature at the region indicated by A_I or A_{II} reflects possibly desorption of the encapsulating thiolates before coalescing of the particle cores. The temperature rise at the region indicated by B_I or B_{II} may then reflect a combined effect of coalescing and growth of the nanoparticles and re-deposition of the thiolates. Desorption of the thiolates is an endothermic process because it breaks the Au-S bond, and consequently leads to the temperature fall. In contrast, particle coalescence and re-deposition of the thiolates involve the formation of new bonds, and thus raise the temperature. The endothermic/exothermic processes are important to the actual temperature measured because they exhibit an impact to the temperature profiles. The associated temperature changes are however relatively small (5~10 ^{0}C) in comparison to the overall heating temperature. The fact that the nanoparticles evolved under these heating conditions are stable for months serves an indication of encapsulation of the nanoparticles by the thiolate shell. We next present both microscopic and spectroscopic data for characterizations of the morphological and structural properties of the evolved nanoparticles.

Characterizations of the Morphological and Structural Properties. The heating-evolved nanocrystals were characterized by a number of techniques: TEM for particle size and shape, UV-Vis for size evolution, IR for thiolate shell structures, and XRD for crystallinity properties. The results of these characterizations consistently revealed a sharp contrast for the nanoparticles before and after the temperature-induced evolution.

Transmission Electron Microscopic Imaging. For the 2-nm particles synthesized according to the standard two-phase protocol, there are already extensive TEM characterizations reported in the recent literature. [3-12,16, 19] Our own TEM data showed an average core size of ~2.0 nm with ~80% populations at 1.5 to 2.5 nm range. [16] The particle sizes appeared non-uniform with shapes appearing polyhedrons and truncated octahedrons, the latter of which was predicted to be the most likely shape[25]. In contrast to these morphological features, several striking observations are evident for the nanoparticles evolved from the heating treatment, as shown in Figure 3 for a representative TEM image. Clearly, the TEM image displays an increased core size with a narrow distribution in which more than 90% populations are at 4.7 to 5.7 range and they average to 5.2 nm. The size distribution of such evolved particles is much narrower than the 2-nm particles before heating treatment. A close examination of the particle shapes reveals a predominant presence of faceted particles. Based on more than 10 samples, a small percentage of the particles seems to exhibit "hexagon" outlines with some plate-like features as hinted by the uniform color across the particles. Such faceting properties are suggestive of an evolution in shapes.

These features are remarkable because the evolution leads to well-defined morphology both in size and in shape (or facets).

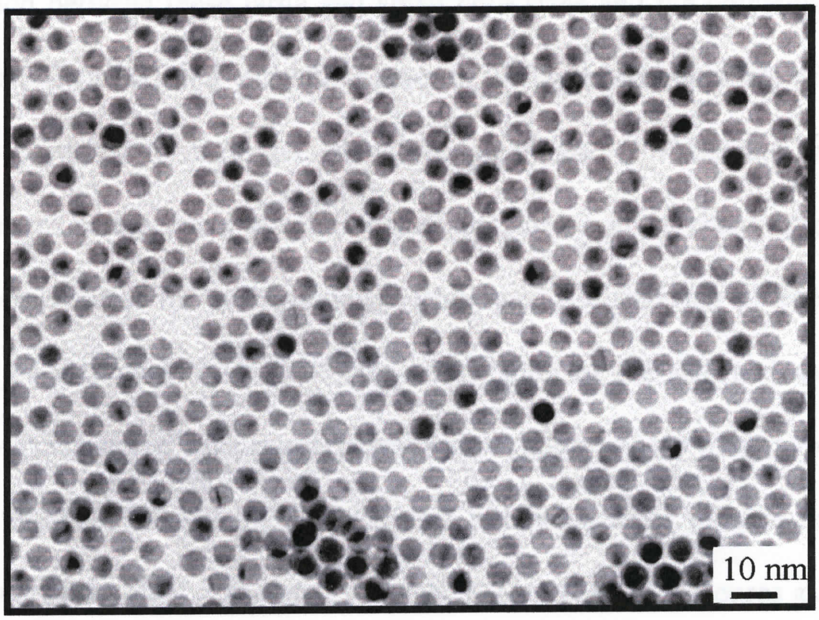

Figure 3. TEM micrograph of a DT-encapsulated Au nanoparticle sample prepared by the heating treatment of a 2-nm particle solution at 138 ^{o}C that was followed by further heating at ~110 ^{o}C for 12 hrs duration.

As an approximate estimate of the number of particles involved in forming the larger-sized particles, we consider a mass balance model in which the large-sized core is a simple coalescence of the small-sized cores. This model then relates the average particle radius (assuming spherical) by the relationship:

$R_L = N^{1/3} R_S$ ....(4)

where R_L is the radius of the large-sized particles, R_S radius of the small-sized particles, and N the number of smaller particles. The calculation based on eqn. 4 yields N = ~15 for a size evolution from the 2-nm to the 5-nm cores. The involvement of such a significant number of particles in the coalescence is consistent with the early description of the necessity of preconcentration condition before the heating treatment. As will be further evidenced by XRD data, these coalesced particles are in fact highly crystalline cores. We believe the distinction between these large and small core sizes and the corresponding shape evolution are inherently associated with differences in the chemical potentials of the particles in which smaller particles have larger chemical potentials. While not reported for thiolate-encapsulated nanocrystals in solutions, temperature-induced changes in size and morphology have been reported for quasimelting, coalescence and sintering of fine metal or metal oxide crystals or particles.[35, 27-28, 36-37] The observation of the size and shape evolution for the thiolate-encapsulated Au nanoparticles in the solution phase may involve similar processes, but the ultimate balance of the chemical potentials must involve the desorption and re-adsorption of the shell components and the coalescence of the cores as the driving forces for the eventual size and shape.

These 5-nm nanocrystals also exhibit a remarkable long-range ordering feature upon casting the particle solution onto a TEM grid and evaporating the solvent. Such type of self-organization is reflected by large domains of long-range two-dimensional ordered arrays with a hexagon-type arrangement (Figure 3). Similar long-range orders have recently been reported for alkanethiolate-encapsulated gold nanoparticles that were prepared without heating treatment, for examples, by fractionalized dodecanethiolate-encapsulated gold particles,[25] by gas-phase synthesis followed by solution-phase encapsulation,[38] and by two-phase synthesized gold particles coated with quaternary ammonium bromide ion pairs.[10] Our observation serves as an intriguing example for the long range ordering of the thiolate-encapsulated nanocrystals prepared by the heating treatment. In an excellent agreement with the notion that the encapsulating chains are likely interdigitated between opposing alkyl shells,[6,15,39,25] the determined average core-core (edge-to-edge) distance, ~1.5 nm, is indeed close to the expected chain length of DT (1.4~1.5 nm). Effects from both van der Waals attractions of the encapsulating shells and the core shape are believed to be responsible for the formation of ordered arrays.

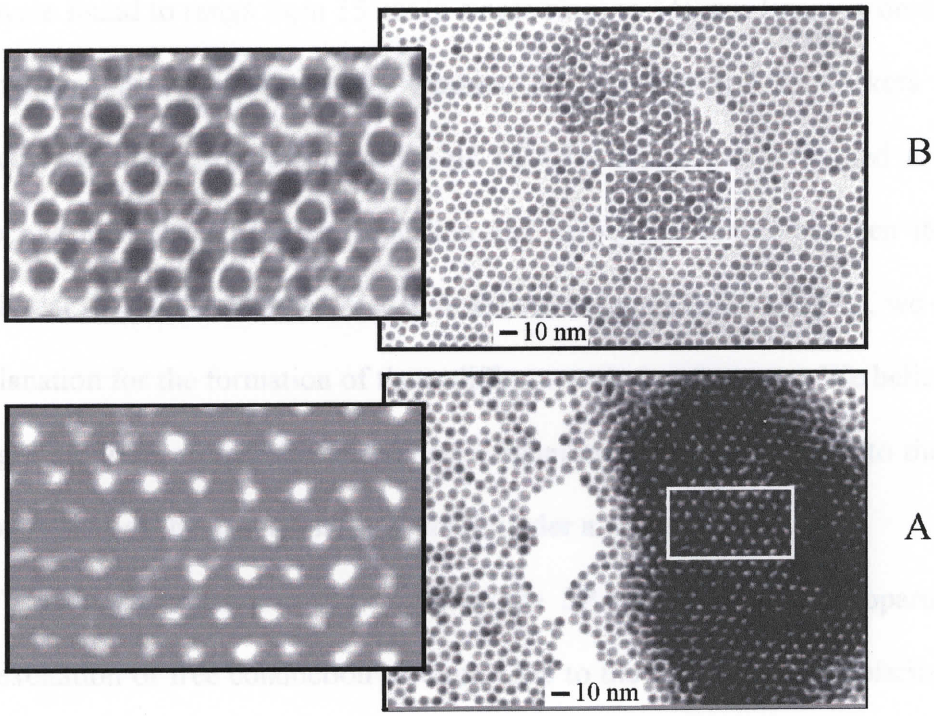

Figure 4. TEM micrographs of two types (A and B) of 3D-ordered domains of the DT-encapsulated nanoparticles evolved from the heating treatment at 138 ^{0}C that was followed by 5 hrs duration of heating at ~100 ^{0}C. The left representations are the magnified views of the indicated areas.

Small areas of 3D organization features are also observable in Figure 3. Larger domains of the 3D ordering features were in fact observed depending on the preparation conditions including the time length of the heating treatment. Figure 4 shows two types of domains for a nanoparticle sample evolved from the heating treatment at 138 ^{0}C that was followed by 5 hrs duration of heating at ~110 ^{0}C. In Figure 4A, we observe a domain in which a regular hexagonal ordering occurs for the second nanoparticle layer (see the magnified view). The domain sizes were found to range from 50 nm to 300 nm. In figure 4B, we observe another completely different domain in which the second nanoparticle layer exhibits a ring-structured ordering (see the magnified view). The domain sizes of this type of ordering were found to range from 15 nm (a single ring) to 150 nm (many ordered rings). A similar ring-type feature was recently reported by Schiffrin and co-workers [10] for gold nanoparticles synthesized in the presence of TOABr, which was attributed to the charge balance between local electrostatic repulsion and dispersion forces between the particles. While a similar mechanism may be operative for the ordering in our samples, we do not have a full explanation for the formation of these different ordering features. We believe that part of the origin for these remarkable 2D/3D self-organizations may be linked to the shape and faceting properties of the nanocrystals, which is under a further investigation.

UV-Visible Measurement. The origin of the SP band for gold nanoparticles is the coherent excitation of free conduction electrons due to the induction of a polarization of the electrons with respect to the ionic core of the particle by the electrical field of light [29]. The net charge difference occurs at the nanoparticle surface leads to a dipolar oscillation of the electrons. It is not originated from interband transition. In a semiconductor, the energy level difference between completely filled valence band and the empty conduction band leads to interband transition, in the order of a few eV that increases with decreasing particle size. In a metal, the conduction band is half-filled, and there is an insignificant energy difference between different energy levels so that the interband transition is only observed when the particle size is very small, in the order of a hundred atoms. A 1-nm sized gold nanoparticle consists about 30 atoms and has an energy spacing of about 167 meV, exceeding the thermal energy (kT~26meV). The LUMO-HOMO bandgap is about 1.7 eV. SP band arises from the coherent excitation (or oscillation) of free electrons in the conduction band due to the small particle size effect. It is also due to the surface effect it alters the boundary conditions for the polarizability of the metal and thus shifts the resonance to optical frequencies. The molar absorptivity can be in the order of $\sim 10^9$ $M^{-1}cm^{-1}$ for a 20-nm particle which is 3~4 orders of magnitude higher than many organic dye molecules. Our $Au_{5\text{-nm}}$ nanoparticles showed a molar absorptivity of $\sim 10^6$ M^{-1} cm^{-1}.

The SP electron excitation is dependent on particle size. A change in absorbance or wavelength provides a measure of particle size, shape and aggregation properties. For a very small particle (< 2 nm), the SP band is very weak or broad and almost completely disappears because the plasmon oscillation is strongly damped due to the very small electron density in the "conduction" band. As particle size increases (<20nm), the SP band becomes strong because the conduction electron density increases. For larger sized particles (>20 nm), the SP band even show red shift and broadening, which can be qualitatively and quantitatively explained by Mie's theory [39]. The change of the SP optical property thus offers an effective means to assess the evolution of gold nanoparticles, which can be measured by UV-Vis spectrophotometry.

Figure 5 shows a set of UV-Vis spectra sampled at different times during the heating process. The spectrum for the 2-nm sized particles in hexane displays an identifiable but weak SP band envelope around ~515 nm (*a*). The shape and position of this band are in agreement with those previously reported for particles of similar sizes synthesized according to the two-phase method.[8,15] Upon prolonged heating of the solution at temperatures bellow

110 ±5 ^{0}C (see Figure 2), no significant change in the shape and position of the SP band was observed. This result confirmed the remarkable stability of the nanoparticles at the temperature before the onset of the evolution.

In contrast, the spectra sampled after the solution temperature reaches 138 ±2 ^{0}C exhibited an increased intensity for the SP band at 520-nm (*b-d*). The intensity of this band increased with the time length of a continuous heating at a lower temperature (~110 ^{0}C)

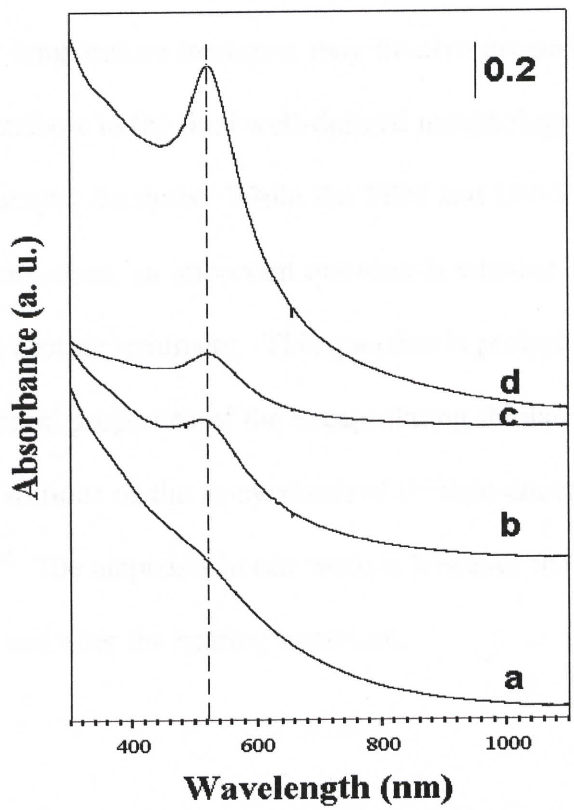

following the evolution, whereas the peak position remained unchanged. The general feature of the band is in agreement with those obtained for 4-6 nm sized Au nanoparticles synthesized via controlling the thiol to Au ratios.[15] Importantly, the increased intensity of the

SP band, without an apparent shift in energy, is indicative of an increase in core size, a well-documented optical property for gold particles of different core sizes in this size range.[8,10,40]

We further note that a prolonged heating at or above the evolution temperature of 138 ±2 °C shifts the SP band to higher wavelength associated with a further growth of the particles. Because of the less-soluble or insoluble nature of the resulting particles in the organic solvent, the study will be described elsewhere. In contrast, a prolonged heating at lower temperatures (<120 °C) following the evolution showed little impact to the peak position of the SP band except a further increase of its intensity to a certain degree. We believe that this lower temperature treatment may involve processes of particle shaping and homogenizing that contribute to the final well-defined morphology and monodispersity.

Infrared Spectroscopic Analysis. While the TEM and UV-Vis data have confirmed the evolution of particle core sizes, an important question is whether the integrity of the organic shell is affected by the heating treatment. This question is probed using IR spectroscopy that characterizes the structural properties of the encapsulating thiolate shells. We note here that extensive IR characterizations of the as-synthesized thiolate-encapsulated gold nanoparticles have been reported.[13,15] The emphasis in our work is however the comparison of the thiolate shell structures before and after the heating treatment.

Figure 6 shows two un-processed IR spectra for the 2-nm (*a*) and the 5-nm (*b*) Au nanoparticle powder samples in KBr pallets. The overall similarity in both high and low energy regions suggests the absence of major structural decomposition or transformation. There are however two main structural differences in terms of the shell packing/ordering and the core electronic properties.

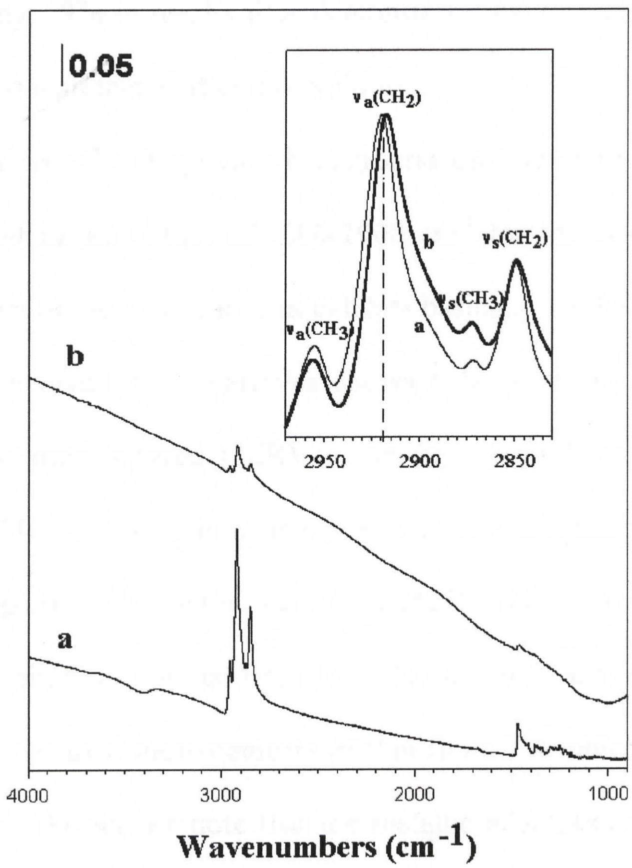

Figure 6. FTIR spectra of powder samples in KBr pallets for nanoparticles of the 2-nm (*a*) and the 5-nm (*b*) core sizes. The insert represents a normalized view of the two spectra in the C-H stretching region with the asymmetric and symmetric stretching bands of methylene and methyl groups being indicated.

First, a close examination of the C-H stretching region (Figure 6, insert) provides the diagnostic information about the ordering properties of the alkyl chains. While the bands corresponding to methyl stretching (2955 and 2872 cm^{-1}) show little change, a shift to lower wavenumbers is identified for the asymmetric and symmetric methylene stretching bands from the 2-nm (2920 and 2850 cm^{-1}) to the 5-nm (2917 and 2948 cm^{-1}) particles. The observed shift is reproducible as confirmed by at least 10 sets of powder samples. Similar observations were reported for systems involving thiolate monolayers on planar[39] and on nanocrystal gold,[8,10] where such a shift was linked to the more crystalline nature[41] of the monolayer packing. These results thus demonstrate that the integrity of the encapsulating thiolate structure is maintained after the evolution.

Secondly, a significant spectral background difference between the 2-nm and 5-nm particles is evident in the region of 4000-1000 cm^{-1} for the un-processed powder spectra. While the spectrum of the 2-nm particles exhibits basically flat background in this region, the spectrum of the evolved 5-nm particles shows a large absorption feature. It is in fact extended into the near infrared (NIR) region (up to 9000 cm^{-1}, as determined by NIR measurement). This property is characteristic of the conductive metallic adsorption for larger-sized nanoparticles in continuous solid state.[42] This type of feature has recently been demonstrated for thin films derived from 10 to 20 nm sized bare gold particles,[43] and has also been observed in our own measurements of thin films assembled from the heating-evolved nanocrystals.[17-20] We further note that the metallic adsorption in the IR-NIR region also depends on the preparation of the samples. The spectral difference could be minimized if the sample pallet was prepared by first dissolving the particles in hexane solution, mixing it with KBr powders and allowing solvent evaporation before grounding into a pallet. In addition, we measured IR spectrum of the 5-nm particles in solution (hexane), and the data did not reveal any indication of a rising IR-NIR background, supporting further that the spectral feature was arising from the solid state sample properties. This spectral feature can be attributed to the effective breaking of the continuous shell contacts between the individual nanoparticles in the sample in comparison with the nanoparticle powder samples.

X-Ray Diffraction Analysis. Another critical question concerns with whether the large-sized particle is a simple aggregation of the small sized particles or a larger crystalline core. This issue was examined using XRD technique that was proven useful for characterizing the crystallinity and size of nanocrystals.[25,43]

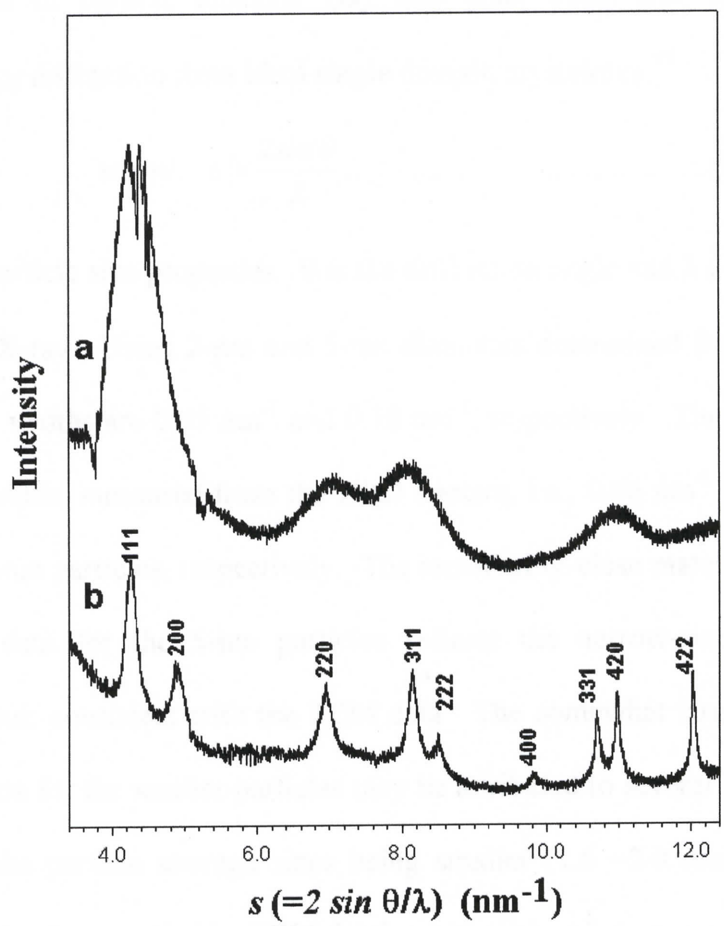

Figure 7. X-ray diffraction of powder samples of the 2-nm (*a*) and the 5-nm (*b*) Au nanoparticles.

Figure 7 shows the XRD spectra for 2-nm (*a*) and the 5-nm (*b*) particles. Important evidence on the crystallinity properties emerges from the spectral comparison. First, the observation of the expected diffraction patterns demonstrates that both the 2-nm and 5-nm particles are crystalline cores. As indexed, the 5-nm crystal cores exhibit a well-defined crystallinity that approaches that of bulk gold.

Secondly, the peak width is much narrower for the 5-nm particles than for the 2-nm particles. Such a difference is indicative of the difference in particle sizes because it is known that smaller particle size exhibits a larger diffraction peak width.[25,43] Based on Scherrer correlation of particle diameter (D) with peak width (Δs, full width at half maximum) for Bragg diffraction from ideal single domain crystallites [43],

$$\Delta s = 0.9\frac{1}{D} \qquad where \quad s = \frac{2\sin\theta}{\lambda} \quad \ldots\ldots\ldots\ldots\ldots\ldots (5)$$

we can assess the particle size properties. θ is the diffraction angle and λ (= 0.154 nm) is the wavelength of the X-ray. Using 2-nm and 5-nm diameters determined from the TEM data, the calculated peak widths are 0.45 nm^{-1} and 0.18 nm^{-1}, respectively. These values are very close to the peak widths measured from the XRD spectra, i.e., 0.66 nm^{-1} and 0.18 nm^{-1} for the 2-nm and the 5-nm particles, respectively. The remarkably-close match of the theoretical and experimental data for the 5-nm particles reflects the narrow-sized feature of the nanoparticles, a result consistent with the TEM data. The somewhat larger deviation from the experimental data for the smaller particles may be attributed to several reasons, including the possibility of the particle average sizes being smaller (1.6 ~2.0 nm) and the lack of monodispersity in size (as revealed by TEM data).

The XRD data thus confirm that the heating-evolved large-sized particle has a highly crystalline core, rather than a simple collection of the smaller precursor particles. The data also showed remarkable consistency with the TEM data in terms of sizes and monodispersity.

Part II. Manipulation of the Thermally-Activated Core-Shell Reactivities

Having demonstrated the viability of the thermally-activated processing strategy, we further expand processing strategy by investigating the manipulation of the core-shell nanochemistry. In this part, we describe three closely-related manipulation approaches in terms of the core-shell chemistry. First, a solution annealing ("baking") effect is investigated to further increase the size and shape monodispersity of the thermally evolved particles. Second, the dependence of the evolution temperature on the chain length of the encapsulating thiolates is studied for assessing processing parameters. Third, the dependence of the thermal evolution on the nanoscrystal core composition is investigated to assess the impact of the re-sizing or re-shaping to the core-shell properties.

Annealing Effect on the Evolved Size and Shape

The "solution annealing" refers to a treatment procedure by which the temperature of the solution, upon the observation of a solution color change at the evolution temperature, was lowered to ~100^0C and maintained for a certain time duration. An additional solution of encapsulating thiols (~100 mM) was also added to the solution to ensure re-encapsulation during annealing. Such an annealing treatment was found to affect the size and shape homogeneity of the resulting nanoparticles with remarkable effectiveness. Figure 8 shows a representative TEM image of the DT-capped Au nanoparticles evolved from such type of annealing treatment. The image of the precursor 2-nm particles is inserted for comparison. Clearly, the evolved nanoparticles show dramatic changes in size, shape and homogeneity in comparison with the precursor nanoparticles, due to a combination of the heating-induced initial evolution and the subsequent annealing-led further re-shaping and re-sizing effects.

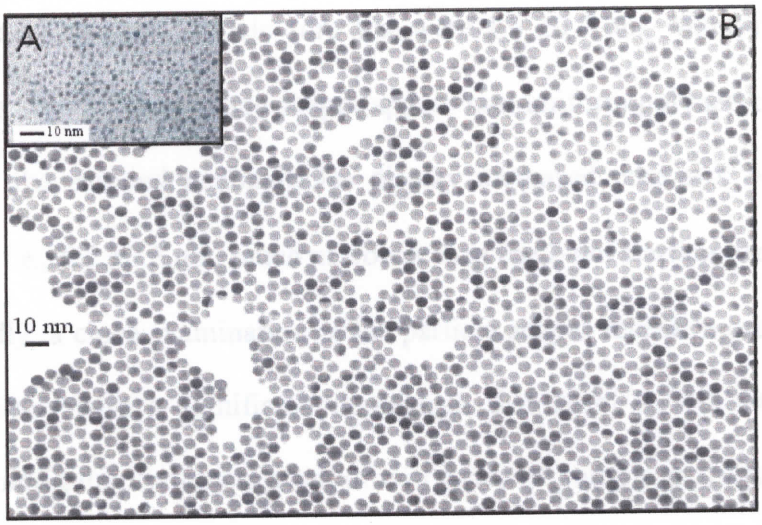

Figure 8. TEM micrographs of DT-encapsulated Au nanoparticles prepared by solution annealing process in the presence of excess DT following the thermally-activated size evolution. The insert shows the TEM image of the precursor nanoparticles.

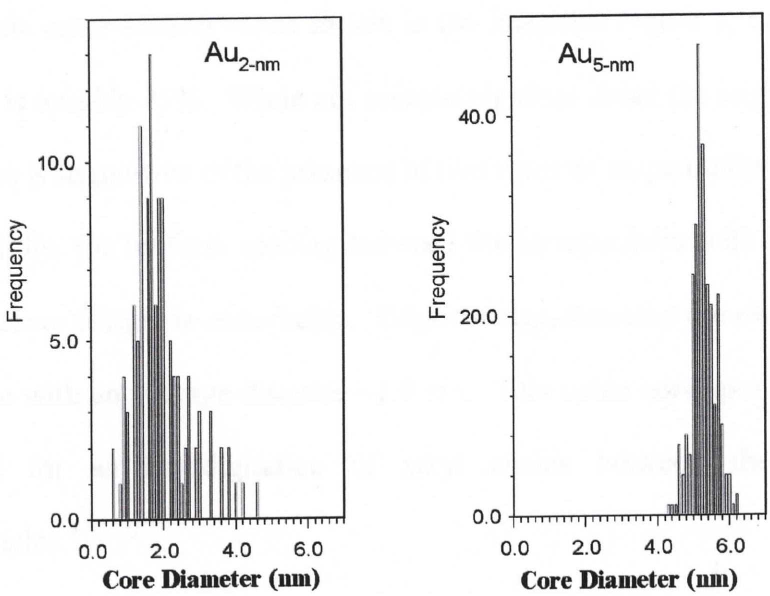

Figure 9. Histograms of the nanocrystal core sizes comparing the precursor (a) and the evolved product (b). The data were determined from the TEM image of Figure 8

Several morphological changes are evident. First, the size distribution is strikingly narrow, as shown in Figure 9 by the contrast of the size distribution histograms for both nanoparticles. The 2-nm particle core size were 1.9 ±0.7 nm, which is consistent with data reported recently [15]. The particle shapes appear non-uniform polyhedrons. In sharp contrast, the data for the evolved nanoparticles display increased core size with very narrow size distribution, i.e., 5.2 ±0.3 nm, much narrower than the 2-nm starting particles.

Secondly, a close examination of the particle shapes reveals a predominant presence of faceted particles with a significant percentage that seem to exhibit "hexagon" outlines. Particularly intriguing is the presence of two types of particle morphologies as reflected by the darkness of the particles in the TEM image. While most particles display plate-like features as hinted by the uniform gray color across the particle, a number of particles exhibit a "3D" morphology as reflected by the distinctive darkness of the particles. On the basis of the particle cross-section views shown in the image of Figure 8, the percentage of the dark particles is roughly 25%. While not completely clear about the origin, we believe that such a difference is suggestive of the presence of two types of shape outline.

Thirdly, the uniform spacing between the nanoparticles with a predominant hexagonal packing array feature is remarkable. Edge-to-edge distances are estimated to range from 0.7 to 1.4 nm with an average distance ~1.0 nm. This value corresponds closely to the distance expected for an interdigitation of alkyl chains between shells of the neighboring nanoparticles [3].

In comparison with recent data showing size and shape evolution of nanoparticles upon heating treatment [16], the above annealing-produced morphological features constitute clear evidence for the existence of a further re-sizing and re-shaping effect for the evolved particles under the annealing process. While the mechanistic details remain to be investigated, we believe the reshaping or re-sizing that minimize the chemical potentials followed by competitive re-encapsulation of thiolate shells under the annealing condition. The latter can be in an analogy to thermal annealing of solid samples. The key distinction is the involvement of a series of chemical processes such as thiolate encapsulation, desorption and re-encapsulation, during which the nanocrystal facets and corners are further developed into energetically-more favorable states. Based on these qualitative considerations, we expect that manipulations of the core composition, shell structures and solution components should have profound impacts on the evolution reactivities and interfacial energies of the thermally-activated core-shell nanoparticles, which are discussed next.

Chemical Manipulation of Core-Shell Reactivities in the Thermal Evolution

Effects of two types of structural manipulations, i.e., chain length of the thiolate shell and composition of the nanocrystal core, on the core-shell reactivities in the size and shape evolutions are investigated to assess their viability for controlling the core-shell reactivities. To gain insights into these effects, three different sets of samples were studied, each with varied characteristics in the core-shell structure or composition. The first set involved Au nanoparticles with the difference in chain length for the encapsulating thiolates, including BT, DT and HDT. The second type involved samples capped with thiolates of one chain length in the presence of thiols of another chain length. The third type involved gold alloy nanoparticles, gold-silver (Au-Ag) and gold-platinum (Au-Pt).

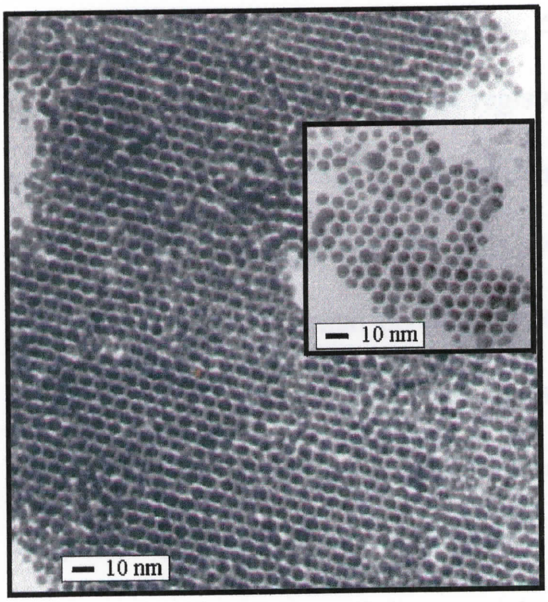

Figure 10. TEM micrographs of the nanoparticle product in two domains: two-layer and one-layer (insert). The product was evolved from HDT-encapsulated Au nanoparticles

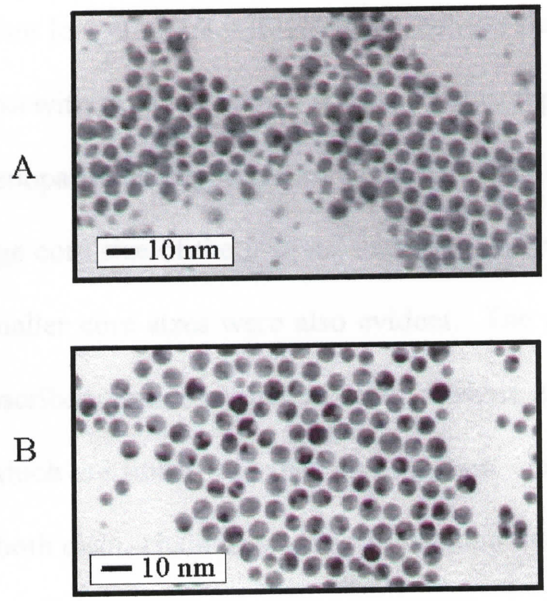

Figure 11. TEM micrographs of the products evolved from DDT-capped Au-Ag (A) and DT-capped Au-Pt (B) nanoparticles

The thermally-activated evolution in particle sizes for these samples is shown by a set of representative TEM images. Figure 10 shows the result of a Au nanoparticle system with HDT thiolates encapsulation, whereas Figure 11 display the results of two alloy nanoparticle systems, Au-Ag (A) and Au-Pt (B). These samples were collected from the heating solutions upon indication of the size evolution without an extensive annealing treatment. Clearly, all samples showed the size evolution to a core size range of 5~7 nm. Domains of hexagon-type packing for a one-layer nanoparticles can be identified for each sample, though the domain sizes vary from sample to sample preparations. The feature is consistent with those previously reported for DT-capped nanoparticles [16]. Interestingly, a long-range ordering with stripe-like array feature can also be observed in a two-layer domain for the Au nanoparticles capped with long-chain thiolates (HDT) (Figure 10). Based on the elongated dimension feature of the particles in the array (i.e., 5.3 nm long and 3.8 nm wide), we believe that the second layer adopted a slight offset registration with respect to the first layer. Other types of registration were previously reported for nanoparticles capped with DT and other shells [16,10,15]. For the alloy nanoparticles, the average core size of the evolved nanoparticles was in the 5-6 nm range. A small percentage of smaller core sizes were also evident. The origin could be due to the lack of annealing as described earlier or due to other possible effects involving two different core compositions, which are under a further investigation. Further insights are provided by studies of effects of both chain-chain interaction of capping thiolates and core-core interaction of alloy particles.

Effect of Shell Structures. To demonstrate structural effect of the chain length of the capping alkanethiolates, we report mainly the results from three chain length systems including BT, DT and HDT. The basis for the assessment of the chain length effect on the observed evolution temperatures and structural properties of the resulting nanoparticles is the difference in binding energies of alkanethiolates to the particle. While Au-S bonding is identical for the three chain lengths, the contribution of a cohesive energy due to chain-chain interactions determines the overall binding strength. As a result, the thermal stability and the core-shell reactivities for the encapsulation and re-encapsulation can be manipulated by varying the chain length.

Figure 12 shows a set of UV-Vis data comparing the Au-BT, Au-DT and Au-HDT nanoparticles before and after the heating-induced evolution. The optical absorption band is originated from the surface plasmon (SP) resonance of the nanoparticles [15,40]. Except for Au-BT system which formed insoluble product, both Au-DT and Au-HDT showed similar change of the SP band, which is consistent with the evolution of the particle sizes as revealed by the TEM data (Figure 10). The spectrum for the evolved Au-BT sample was taken in between the observation of the initial evolution product and the observation of the eventual formation of the insoluble product, revealing a small hint of the SP band from a small fraction of the particles that were soluble.

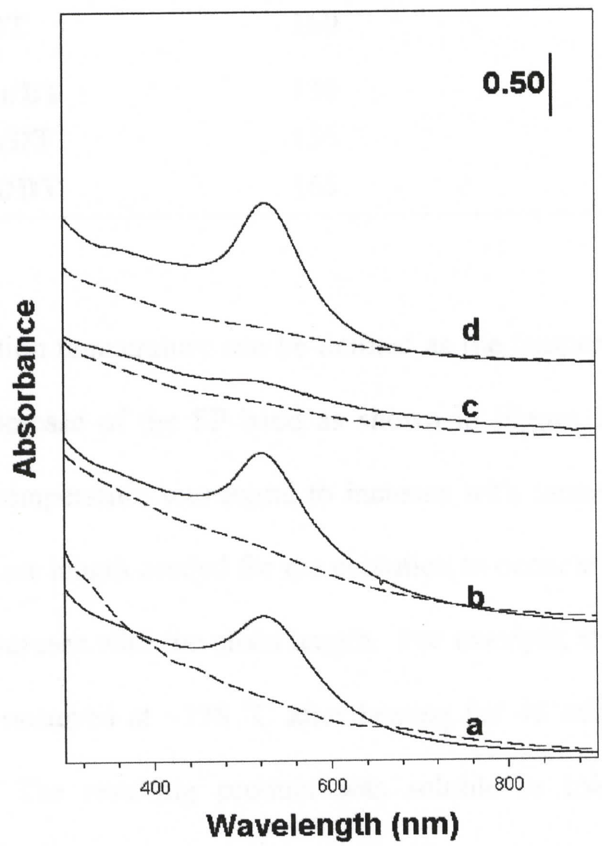

Figure 12. UV-Visible spectra comparing the Au nanoparticle samples before (dashed lines) and after (solid lines) the thermally-activated size and shape evolution. (a) HDT-capped Au, (b), DT-capped Au, (c) BT-capped Au, (d) BT-capped Au evolved in the presence of HDT

The dependence of the evolution processes on the chain length of the encapsulating thiolates is reflected by the different values of the evolution temperature and the associated time length, as summarized in Table 1.

Table 1. A comparison of the evolution temperature (T_E) and the approximate time length (t_E) to reach T_E for the thermally-activated evolution of different core-shell nanoparticle samples

Sample	Thermally-activated Evolution	
	$T_E(^0C)$	t_E (min)
AU/BT	130	30
Au/DT	138	45
Au/HDT	160	65
Au/BT →Au/BT	130	30
Au/Ag(1:4)/DT	155	60
Au/Pt(1:1)/DDT	165	50

The evolution temperature can be defined as the temperature at which there is a color change or an increase of the SP band as shown in Figure 12 for the heated nanoparticle samples. This temperature was found to increase with increasing chain length of the shell thiolates. The time length needed for the evolution to occur at constant bath temperature was also shown to increase with the chain length. For example, the evolution temperature of the DT-capped Au occurred at ~138 ^{0}C after heating for 45 minutes at a bath temperature of 150^{0}C-160^{0}C. The resulting product was soluble in toluene with a deep red color distinctively different from the dark brown starting particles. Importantly, a comparison of the data for the nanoparticles capped with shorter or longer capping thiolate chain length reveals remarkable differences in both temperature and time length. For example, Au capped with BT showed color change at ~125 ^{0}C upon heating for about 30 minutes. This change was however quickly followed by the formation of an insoluble product. In contrast, nanoparticles capped with HDT exhibited the color change to a deep red at ~155^{0}C after about 60 mins of heating in the same oil bath. Clearly, the evolution temperature and the time length increase with increasing chain length of the capping alkanethiolates (Table 1). In other words, a higher temperature is required for the evolution of nanoparticles capped with thiolates of longer chain structures than those with shorter chain thiolates. It is important to note that the time lengths reported do not provide any kinetic assessment on the evolution, rather an assessment of energy needed to achieve the evolution temperature.

These results are qualitatively consistent with both an energetic consideration and experimental thermochemical data reported for the core-shell nanoparticle systems. Energetically, more energy supply is needed to desorb the thiolates before the core-core coalescence can occur. Consider, for example, the cohesive energy of the alkanethiolate shells on Au. It is well known that for monolayer assembly on gold surfaces, thiolate chains are interdigitated via Van der Waals interaction. Such a cohesive energy is estimated to be about 1.0 kJ/mole -(CH_2)- [45]. This consideration qualitatively suggests that the increase of desorption energy with increasing the chain length of the capping thiolates. Recent differential scanning calorimetry data obtained for Au nanoparticle systems with thiolate encapsulation of different chain lengths have indeed shown that the order-disorder transition temperature increases with increasing chain length [3,15,44,] consistent with melting of crystalline alkane hydrocarbons. Our data are thus strong evidence that the chemical reactions involve thermally-activated thiolate desorption in the encapsulating shell.

Re-encapsulation of the evolved nanocrystal cores constitutes another part of the chemical reactivities, which is essential to protect the coalescing particles from forming uncontrollable large aggregates. DT and HDT are clearly effective in this regard, as demonstrated by the well-defined sizes and shapes of the resulting particles. In contrast, the formation of insoluble products for heating the nanoparticles capped with BT is suggestive of the ineffective re-encapsulation by the shorter chain length at the evolution temperature. As a result, the coalescing particle cores further aggregate into insoluble larger particles. In view of the demonstrated importance of the shell encapsulation, we envision that the manipulation of the solution thiol composition should directly affect the re-encapsulation process. This is demonstrated next by an experiment involving heating the nanoparticles capped with shorter chain thiolates in the presence of thiols of long chain length.

Starting with Au nanoparticles capped with BT, the solution was first heated to the evolution temperature and followed by an addition of a small aliquot toluene solution of HDT. Upon further heating, the solution showed a clear color change towards deep red and soluble product. Importantly, as opposed to the formation of insoluble product in the absence of HDT component, the product in the presence of the HDT was now soluble in the heated solution up to ~180^0C. The temperature for Au/BT $\rightarrow$ Au/HDT was in fact close to the evolution temperature for the nanoparticles capped with HDT as described earlier (Table 1). The UV-Vis data for the evolution of the BT-capped Au in the HDT-containing solution is included in Figure 12. In comparison with data for the evolution products for Au-DT and Au-HDT nanoparticles, the SP band for the Au-BT product is now comparable. The greater affinity of the long chain HDT towards gold than that of BT is responsible for the re-encapsulation, ensuring that the resulting particles were not subject to a further aggregation. The role of solution thiol composition for the eventual re-encapsulation is similar to the recent finding on the importance of the highly hydrophobic and polar TOA^+ species in the size and shape evolutions [16]. The combined results demonstrate thus that the thermally-activated evolution indeed involves a series of core-shell reactivities, including the initial desorption of the shell, the coalescence of the gold clusters into larger particles, and the eventual re-encapsulation of the particles, as have been schematically illustrated in scheme1.

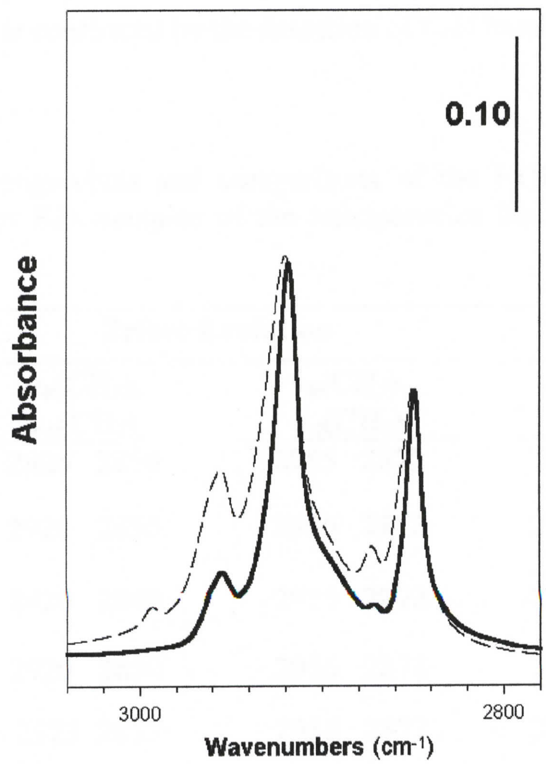

Figure 13. FTIR spectra of powder samples in KBr pellets for the product evolved from the HDT-encapsulated Au nanoparticles (Dashed line: before evolution). The C-H stretching region for the asymmetric and symmetric stretching bands of methylene and methyl groups is shown.

FTIR characterizations probing the capping shell structures of the evolved products provided further structural evidence for the re-encapsulation of the thiolate shell structures, as shown by a representative set of FTIR spectra in Figure 13. The C-H stretching bands are listed in Table 2. First, the overall spectral features for the alkanethiolate encapsulation remain unchanged before and after the evolution, demonstrating the structural integrity.

Secondly, a shift of the methylene stretching bands to lower energy by 2~6 cm^{-1} is observed for the evolved particles, indicative of a more crystalline packing structure of the alkanethiolates. The results are consistent with previous data on larger-sized nanoclusters [23]. And lastly, the re-encapsulation by HDT for heating Au/BT in the presence of HDT (i.e., Au/BT → Au/HDT) is confirmed by the detection of C-H bands diagnostic of HDT thiolates.

Table 2. Mode assignments and comparisons of the FTIR bands (cm^{-1}) in the C-H stretching region for KBr-samples of the nanoparticles before and after the thermally-activated evolution.

Sample	Before Evolution		After Evolution	
	$\nu_a(CH_2)$, $\nu_s(CH_2)$	$\nu_a(CH_3)$, $\nu_s(CH_3)$	$\nu_a(CH_2)$, $\nu_s(CH_2)$	$\nu_a(CH_3)$, $\nu_s(CH_3)$
Au/BU	2926 2850	2955 2872	2926 *	2955 2870
Au/DT	2920 2850	2955 2872	2917 2848	2956 2965
Au/HDT	2920 2849	2955 2872	2918 2848	2954 2870
Au/Ag/DT	2920 2850	2955 2872	2916 2847	2955 2872
Au/Pt/DDT	2923 2853	2955 2872	2919 2849	2955 2872
Au/BT→Au /HDT	2922 2850	2955 2873	2917 2848	2954 2869

Effect of Core Composition. Considering differences of surface atomic distribution of nanoparticle cores for thiolate binding and crystal growth during the core-shell reactions or processes, we have examined several nanoparticle systems with alloy core compositions [15]. Figure 14 shows a set of UV-Vis data for two types of alloy gold nanoparticles, i.e., Au-Ag and Au-Pt.

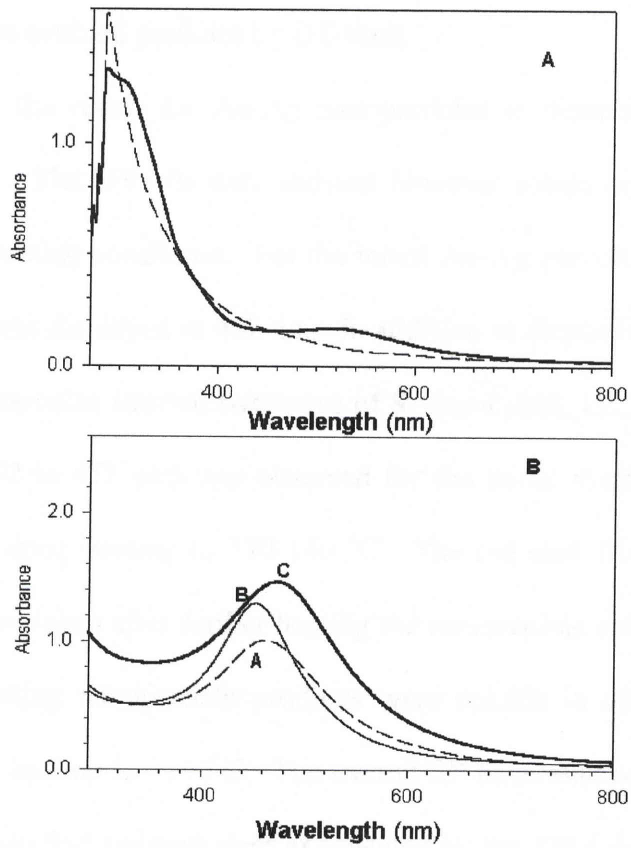

Figure 14. UV-Visible spectra comparing the alloy nanoparticle samples before (dashed lines) and after (solid lines) the thermally-activated size and shape evolution. (A) DDT-capped Au-Pt. (B) DT-capped Au-Ag. For B, curve b is for the sample taken upon the initial heating treatment and curve c is for the eventual product.

For Au-Pt particles, the initial average core size was about 2 nm. Like 2-nm Au particles, no pronounced SP band was observed at the 520 nm wavelength range in initial dark brown Au-Pt solution, though a large band was observed at ~280 nm related to the Pt-component [46]. Upon heating the solution to a temperature of 175 ^{0}C, the particle solution turned red and the UV-Vis spectrum displayed a band at 520 nm similar to that for the 5-nm Au nanoparticles. The result is indicative of a size change for the evolved particles, as confirmed by TEM data (Figure 10B). Clearly, the presence of Pt component in the core did not prevent the particles from core-core coalescence, growth and encapsulation with thiolate shells. FTIR data (Table 2) of the C-H stretching bands are supportive of the re-encapsulation of the evolved particles by DT shell.

Interestingly, the result for Au-Ag nanoparticles is distinctively different from the above observation. The UV-Vis data showed however subtle color and spectral changes depending on the heating conditions. For the initial Au-Ag particles (average core size ~3.5 nm), the SP band was displayed at 462 nm. In addition to displaying an enhancement of SP band, the evolved particles showed two types of SP band shift, i.e., blue and red shifts. The blue shift (from 462 to 451 nm) was observed for the initial evolution, i.e., samples taken after 5-10 minutes upon heating to 130-140 ^{0}C. The red shift (from 451 to 475 nm) was observed for samples taken after further heating the nanoparticle solution to a temperature of ~160^{0}C. The resulting nanoparticle products were soluble in toluene solution, even for samples taken after heating to ~190^{0}C. The overall SP band enhancement is consistent with the size evolution into 5~6 nm core sizes as revealed by the TEM data (Figure 10A). Again, the re-encapsulation of the evolved nanoparticles by DT shell is confirmed by FTIR data (Table 1), which showed the C-H stretching bands comparable to data for the other nanoparticle systems with the same shell encapsulation.

Another interesting characteristic of the evolution for the Au-Ag alloy particles was reflected by the specularly-reflective color of the product in solid state. For example, upon cleaning and drying the evolved nanoparticle product, the particles displayed a reflective greenish color, which was distinctively different from the black or dark gray colors of the other evolved nanoparticles. This characteristic, while not fully understood, is believed to reflect a combination effect of both the increased size and the surface re-distribution of Au and Ag components at the nanocrystal core. The reflective feature is likely associated with a predominant segregation of the silver component surrounding the crystal core. The shell encapsulation of the evolved particles was also confirmed by FTIR data (Table 2).

While the above data demonstrate that the thermally-activated size evolution is operative for alloy core composition, an important question is how the relative distribution of the two components evolve around the nanocrystal core surface, which is important for the catalytic applications of the nanomaterials. It is recently demonstrated [15] that the two components in Ag-Au alloy cluster core are partly segregated. Whether such a segregation is further developed into full segregation as a result of the thermally-activated core-shell reactivities is a subject of our further investigation [47].

Overall, the results, together with our previous results, have shown that the thermally-activated core-shell based evolution is dependent on core composition, shell structure, annealing temperature, and precursor concentration. These dependencies are cooperative, and may not be treated individually for a kinetic assessment. For example, we may expect that the growth rate follows a second-order kinetic behavior in terms of concentration effect. Experimentally, however, the evolution temperature was also changed upon changing concentration. The evolution temperature was observed at 140 ^{0}C for a solution of 12 mM particle concentration, whereas a solution of 1 mM showed an evolution temperature of 120 ^{0}C. By further lowering concentration the temperature stayed close to the solvent boiling point and no particle evolution was evident. The observation is associated with the fact that boiling point rises with increasing mole fraction of the nanoparticles. A complication to the kinetic assessment involves the change of melting point of particles with increasing core size during the evolution. A detailed understanding of this correlation is in progress.

Conclusions and Prospectus

We have described a new strategy towards the processing and manipulation of size, shape and surface properties of nanoparticles and nanostructures. The strategy is explored in two closely-related areas, viability of re-sizing/re-shaping and manipulation of core-shell nanochemistry. In the first area, we have demonstrated that gold nanoparticles of ~2 nm core size synthesized via two-phase protocol could be processed to produce highly monodispersed 5-nm core size. While the data are mostly for the DT-encapsulated gold nanoparticle system, the main findings are representative of most of these thiolate-encapsulated nanoparticle systems. The remarkable evolutions in size, shape, faceting, as well as the encapsulating structural properties are inherently linked to the thermodynamic processes involving core coalescence and growth and shell desorption and re-adsorption. In addition to lowering the melting temperature of the nanoparticles and raising the boiling temperature of the solution, the increase of particle concentration and the presence of hydrophobic and polar tetraoctylammonium component provide the environmental conditions for the morphological evolution.

In the second area, we further expand the thermally-activated core-shell nanochemistry towards processing of size, shape and surface properties by manipulation of annealing condition, shell structures and core composition. The size monodispersity of the evolved particles has been demonstrated to substantially improve by solution annealing process. Experimental data have indicated that the chemical reactivities in the evolution process involve shell desorption, core-coalescence and re-encapsulation. The temperature at which the particles change sizes or shapes was found to be dependent on the chain length of the encapsulating thiolates and the compositions of the nanocrystal cores, both of which play important roles in the size and shape evolution. The dependencies of the evolution temperature on the capping thiolate chain length and the core alloy composition have provided new evidence that the thiolate shell desorption and re-encapsulation are two of the critical processes for the control of the core-shell reactivities.

Most recently, we have explored the construction of functional thin film assemblies from the processed nanoparticles [17-18]. Using atomic force microscopy (AFM), we were able to visualize the nanoparticles thus assembled on a planar substrate. Figure 15 shows a representative AFM image of a thin film assembly derived from $Au_{5\text{-}nm}$ particles crosslinked by 11-mercaptoundecanoic acid linker. While in-depth AFM study of the nanostructures is underway [47], one important feature of the assembled nanoparticles is the individually-isolated character of the assembled particles. This is important because the nanoscale morphology is integrated into macroscopic functional materials.

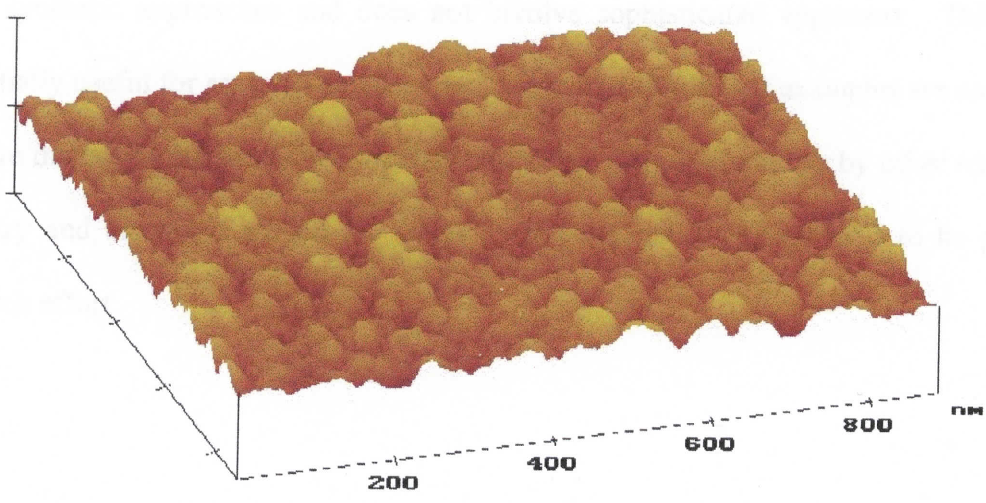

Figure 15. AFM image of a thin film assembly of $Au_{5\text{-}nm}$ nanoparticles. The film is assembled using 11-mercaptoundecanoic acid molecule as crosslinking agent.

We believe that our findings provide new insights into the development of processing pathways for the production of core-shell nanoparticles with well-defined size and shape from pre-formed nanoparticles by relatively simple procedures. The versatile and reproducible procedure may be extended to many other similar composite nanoparticle systems. The synthesis of various thiolate-encapsulated nanoparticles is now well known, but the exploration of the core-shell chemistry is just at the beginning. Indeed, part of our on-going efforts is aimed at further delineation of the controlling parameters in the core-shell chemical processes and reactivities for the desired size and shape manipulations. Such manipulations are critical for developing abilities in the chemical processing of core-shell nanoparticles for potential catalytic and molecular recognition applications. Expansion of this process may also hold the keys to further development of different nanoparticle shapes. It is important to note that the thermal processing of nanoparticles is accomplished in a conventional laboratory setup that involves minimum amount of solvent in comparison with most synthetic approaches and does not involve sophisticated apparatus. This feature is potentially useful for scale up applications. I also like to add that examples are emerging that involve the use of the processing method developed in our laboratory by other researchers in industry and academia around the world. It gives me a greater thrill to be part of this research effort.

References Cited:

1. "Nanotechnology" ed; Gregory Timp; Springer-Veriag New York, Inc. 1999
2. "Nanotechnology Research Directions" ed; M. C. Roco, R. S. Williams, P. Alivisatos, Kluwer Academic Publishers, 2000
3. Hostetler, M. J.; Murray, R. W. *Curr. Opin. Colloid Interface Sci.*, **1997**, *2*, 42, and references therein.
4. Fendler, J. H., Ed. *Nanoparticles in Solids and Solution*; (NATO ASI series) V. 18, Academic Publishers, 1996.
5. Schon, G.; Simon, U. *Colloid Polymer Sci.* **1995**, *273*, 101. and **1995**, *273*, 202.
6. Martin, C. R.; Mitchell, D. T., *Anal. Chem.* **1998,** *70*, 322A.
7. Keating, C. D.; Musick, M. D.; Lyon, L. A.; Brown, K. R.; Baker, B. E.; Pena, D. J.; Feldheim, D. L.; Mallouk, T. E.; Natan, M. J., *ACS Symp. Ser.* **1997,** *679*, 7.
8. Brust, M.; Walker, M.; Bethell, D.; Schiffrin, D. J.; Whyman, R., *J. Chem. Soc., Chem. Commun.* **1994**, 801.
9. Brust, M.; Fink, J.; Bethell, D.; Schiffrin, D. J.; Kiely, C. J., *J. Chem. Soc., Chem. Commun.* **1995**, 1655.
10. Fink, J.; Kiely, C. J.; Bethell, D.; Schiffrin, D. J. *Chem. Mater.* **1998**, *10*, 922.
11. Faraday, M., *Phil. Trans. R. Soc.*, 147, **1857**, 145
12. (a)Terrill, R. H.; Postlethwaite, T. A.; Chen, C. H.; Poon, C. D.; Terzis, A.; Chen, A. D.; Hutchison, J. E.; Clark, M. R.; Wignall, G.; Londono, J. D.; Superfine, R.; Falvo, M.; Johnson, C. S.; Samulski, E. T.; Murray, R. W. *J. Amer. Chem. Soc.* **1995**, *117*, 12537. (b) Mirkin, C. A.; Letsinger, R. L.; Mucic, R. C.; Storhoff, J. J. *Nature* **1996,** *382*, 607. (c) Elghanian, R.; Storhoff, J. J.; Mucic, R. C.; Letsinger, R. L.; Mirkin, C. A. *Science,* **1997**, *277***,** 1078. (d) Freeman, R. G.; Garbar, K. C.; Allison, K.J.; Bright, R. M.; Davis, J.A.; Guthrie, A. P.; Hommer, M. B.; Jackson, M. A.; Smith, P.C.; Walter, D. G.; Natan, M.J. *Science* **1995**, *267***,** 17. (e) Garbar, K. C.; Freeman, R. G.; Hommer, M. B.; Natan, M.J., *Anal. Chem.* **1995**, *67*, 735.
13. Hostetler, M. J.; Stokes, J. J.; Murray, R. W. *Langmuir* **1996,** *12*, 3604.
14. Hostetler, M. J.; Zhong, C. J.; Yen, B. K. H.; Anderegg, J.; Gross, S. M.; Evans, N. D.; Porter, M. D.; Murray, R. W.; *J. Amer. Chem. Soc.* **1998**, *120***,** 9396.

15. Hostetler, M. J.; Wingate, J. E.; Zhong, C. J.; Harris, J. E.; Vachet, R. W.; Clark, M. R.; Londono, J. D.; Green, S. J, Stokes, J. J.; Wignall, G. D.; Glish, G. L.; Porter, M. D.; Evans, N.D.; Murray, R. W. *Langmuir* **1998,** *14*, 17.

16. (a) M. M. Maye, W. X. Zheng, F. L. Leibowitz, N. K. Ly, C. J. Zhong, *Langmuir, 16*, 490, **2000**. (b) M. M. Maye and C. J. Zhong, *Journal of Materials Chemistry, 10 (8),* 1895, **2000**. (c) C. J. Zhong; W. X. Zheng; F. L. Leibowitz; H. H. Eichelberger, *Chemical Communications, 13*, 1211, **1999.** (d) M.M. Maye, W.X. Zheng, F.L. Leibowitz, N.K. Ly, H.H. Eichelberger, C.J. Zhong, in *Nucleation and Growth Processes in Materials***,** Edited by Gonis, A, et al, Mater. Res. Soc. Proc., Vol. 580, E5-39, **2000**

17. (a) F. L. Leibowitz, W. X. Zheng, M. M. Maye, and C. J. Zhong, *Analytical Chemistry*, *71*, 5076, **1999**. (b) C. J. Zhong, W. X. Zheng, F. L. Leibowitz, and H. H. Eichelberger, *Proceedings of the International Symposium on New Directions in Electroanalytical Chemistry II,* The Electrochemical Society, Inc., 225, **1999**. (c) C. J. Zhong; W. X. Zheng; F. L. Leibowitz, *Electrochemistry Communications*, *1*, 72 **1999**.

18. (a) W. X. Zheng, M. M. Maye, F. L. Leibowitz, C. J. Zhong, *Analyst (Communication)*, 125, 17, **2000** (b) W.X. Zheng, M. M. Maye, F. L. Leibowitz, C. J. Zhong, *Analytical Chemistry*, 72, 2190 **2000**.

19. F. X. Zhang, W. Zheng, M. M. Maye, Y. Lou, L. Han, and C. J. Zhong, *Langmuir*, 16, 9639, **2000**.

20. (a) M. M. Maye, Y. Lou and C. J. Zhong, *Langmuir*, 16, 7520, **2000**. (b) Y. Lou, M. M. Maye, L. Han, J. Luo, C. J. Zhong, *Chemical Communications,* 5, 473 **2001**. (c) Y. Lou, J. Luo, M. M. Maye, C. J. Zhong, M. Hepel, *Electrochemistry Communications,* in press.

21. Bond, G. C., Thompson, D. T., *Catal. Rev.*, **1998**, *145*, 124

22. M. M. Maye, J. Lou, C. J. Zhong; manuscript in preperation

23. Mohamed, M. B.; Ismail, K. Z.; Link, S.; El-Sayed, M. A., *J. Phys. Chem. B* **1998,** *102,* 9370. (b) Weisbecker, C. S.; Merritt, M. V.; Whitesides, G. M. *Langmuir* **1996,** *12,* 3763.

24. Yu, Y-Y.; Chang, S-S.; Lee, C-L., Wang, C. R. C.; *J. Phys. Chem. B.* **1997**, *101***,** 6661.

25. Whetten, R. L.; Khoury, J. T.; Alvarez,M. M.; Murthy, S.; Vezmar, L.; Wang, Z. L.; Stephens, P. W.; Cleveland, C. L.; Luedtke, W. D.; Landman, U. *Adv. Mater*. **1996,** *8,* 428
26. Stella, A.; Cheyssac, P.; Kofman, R. in *Science and Technology of Thin Films*, Ed. By Matacotta, F. C. and Ottaviani, G. World Scientific, **1996**, Vol.57, p57.
27. Miki-Yoshida, M.; Tehuacanero, S.; Jose-Yacaman, M. *Surf. Sci.*, **1992**, *274,* 569.
28. Lijima, S.; Ajayan, P. M. *J. Appl. Phys.*, **1991**, *70***,** 5138.
29. Seshadri, R, Subbanna, G. N., Vijayakrishnan, V., Kulkarni, G. U., Ananthan-krishna, G., Rao, C. N. R., *J. Phys. Chem*., **1995**, *99*, 5639.
30. (a) Buffat, Ph.; Borel, J. P., Phys. Rew., A. **1976,** *13*, 2287. (b) Borel, J. P. *Surf. Sci.* **1981**, *106*, 1.
31. Lewis, L.L.; Pablo, J.; Barrat, J-L., *Phys. Rev. B.,* **1997**, *56,* 2248.
32. Atkins, P. E. Ed., *Physical Chemistry*, 3rd Ed., Freeman, 1978, p.171
33. M. J. Hostetler, C. J. Zhong, B. K. H. Yen, J. Anderegg, S. M. Gross, N. D. Evans, M. D. Porter, R. W. Murray, *J. Amer. Chem. Soc.* 1998, **120,** 9396.
34. Bart, E.; Meltsin, A.; Huppert, D. *J. Phys. Chem*. **1994**, *98,* 10819.
35. (a) Ahmadi, T. S.; Wang, Z. L.; Green, T. C.; Henglein, A and El-Sayed, M. A.; *Science* **1996,** *272,* 1924. (b) Wang, Z. L.; Petroski, J. M.; Green, T.C.; and El-Sayed, M. A. *J. Phys. Chem. B*. **1998,** ***102,*** 6145.
36. Jose-Yacaman, M.; Miki-Toshida, M. *Phys. Rev.,* **1992**, *46,* 1198
37. Duff, D. J.; Curtis, A. C.; Edwards, P.; Jefferson, D. A.; Johnson, F. G.; Kirkland, A. I.; Logan, D. E. Angel. *Chem. Int. Ed. Engl*. **1987**, *26*, 7.
38. Andres, R. P.; Bielefeld, J. D.; Henderson, J. I.; Janes, D. B.; Kolagunta, V. R.; Kubiak, C. P.; Mahoney, W. J.; Osifchin, R. G. *Science* **1996,** *273,* 1690.
39. Mie, G., *Ann. Phys*., **1908**, *25*, 329
40. (c) Alvarez, M. M.; Khoury, J. T.; Schaaff, T. G.; Shafigullin, M. N.; Vezmar, I.; Whetten, R. L. *J. Phys. Chem*., B, **1997**, *101*, 3706.
41. (a)Peschel, S.; Schmid, G. *Angew. Chem. Int. Ed.* **1995**, *34,* 1442. (b) Chumanov, G.; Sokolov, K.; Cotton, T. M. *J. Phys. Chem.* **1996,** *100*, 5166. (c)Johnson, S. R.; Evans, S. D.; Mahon, S. W.; Ulman, A. *Langmuir* **1997**, *13*, 51.

42. Brouers, F.; Clerc, J. P.; Giraud, G.; Laugier, J. M.; Randriamantany, Z. A., *Phys. Rev., B*, **1993**, *47*, 666.

43. (a) Schaaff, T. G.; Shafigullin, M. N.; Khoury, J. T.; Vezmar, I.; Whetten, R. L.; Gullen, W. G.; First, P. N.; Gutierrez-Wing, C.; Ascensio, J.; Jose-Yacaman, M. J., *J. Phys. Chem*. B., **1997**, *101*, 7885. (b) Musick, M. D; Pena, D. J.; Botsko, S. L.; McEvoy, T. M.; Richardson, J. N.; Natan, M. J, *Langmuir,* **1999**, *15*, 844.

44. A. Badia, L. Cuccia, L. Demers, L.; F. Morin, R. B. Lennox, *J. Am. Chem. Soc.* 1997, **119,** 2682.

45. (a) R. G. Nuzzo, L. H. Dubois, D. L. Allara, *J. Am. Chem. Soc.,* 1990, **112,** 558. (b) C. J. Zhong, M. D. Porter, *J. Electroanal Chem.,* 1997**, 425,** 147.

46. C. Yee, M. Scotti, A. Ulman, H. White, M. Rafailovich, J. Sokolov, *Langmuir*, 1999, **15,** 4314.

47. M. M. Maye, C. J. Zhong, Manuscript in preparation.

Acknowledgments

I appreciated financial support of this work through the Binghamton University Deans Office Undergraduate Research Award, and the 1999-2000 and 2000-2001 Materials Research Society "Undergraduate Materials Research Initiative" (UMRI) award. I thank my co-workers over the past few years, including Frank Leibowitz, Lisa Israel, Wenxia Zheng, Yongbing Lou, Li Han, David Daniel, Felicia Zhang, Scott Kowalesky, and Jin Lou.

I extend my gratitude to my advisor, Dr. C. J. Zhong, for guidance and support in developing my abilities as a researcher, and for always finding time to answer any questions.

I thank my Friends Tony and Carolyn Clark for their great friendship, and our meaningful conversations.

I would especially like to thank my family. My loving parents for their never showing any doubt in my career choices. I thank my grandparents. And I thank my best friends and siblings; Chris, Mike, Katie and Karen.